Electromagnetic diffraction radiation of a subwavelength-hole array excited by an electron beam

Shenggang Liu, Min Hu,* Yaxin Zhang, Yuebao Li, and Renbin Zhong
Terahertz Research Center, University of Electronic Science and Technology of China, Chengdu 610054, China
(Received 10 November 2008; revised manuscript received 19 June 2009; published 10 September 2009)

This paper explores the physics of the electromagnetic diffraction radiation of a subwavelength holes array excited by a set of evanescent waves generated by a line charge of electron beam moving parallel to the array. Activated by a uniformly moving line charge, numerous physical phenomena occur such as the diffraction radiation on both sides of the array as well as the electromagnetic penetration or transmission below or above the cut-off through the holes. As a result the subwavelength holes array becomes a radiation array. Making use of the integral equation with relevant Green's functions, an analytical theory for such a radiation system is built up. The results of the numerical calculations based on the theory agree well with that obtained by the computer simulation. The relation among the effective surface plasmon wave, the electromagnetic penetration or transmission of the holes and the diffraction radiation is revealed. The energy dependence of and the influence of the hole thickness on the diffraction radiation and the electromagnetic penetration or transmission are investigated in detail. Therefore, a distinct diffraction radiation phenomenon is discovered.

DOI: 10.1103/PhysRevE.80.036602 PACS number(s): 41.20.−q, 41.60.−m, 42.25.Fx, 42.82.Et

I. INTRODUCTION

Subwavelength holes array (SHA) becomes the most attractive research area in modern science and technology for it is of interest to a wide spectrum of scientists, ranging from physicists, opticists, and material scientists because of its very unusual characteristics and potential applications [1–19]. Early in the 60s, SHA was presented by Ulrich [1] as inductive grids in far-infrared frequency region. The theory and properties of SHA have been developed by Chen [2,3] and McPhedran and Maystre [4] in the 70s. Recently, based on SHA, the mimicking surface plasmon modes and their potential applications were presented and experimentally verified [5,7–11,13,20–22]. Scientists pay much attention to the enhanced electromagnetic transmission through the SHA below the cut-off. A large number of papers have been published, and most of them are for the plane wave excited transmission problems with frequency from optics to microwave.

This paper explores the physics of the diffraction radiation and the accompanied electromagnetic penetration or transmission of a subwavelength holes array. It shows that when a line charge of the electron beam is uniformly moving closely parallel to the surface of a SHA shown in Fig. 1, numerous physical phenomena occur involving the diffraction radiation on the both sides of the SHA, and the electromagnetic penetration into or transmission through the holes array as well. The above phenomena are connected to each other to form an entire physical process. The detailed computer simulation is carried out in Sec. II to demonstrate the whole event, and then making use of the integration approach together with relevant Green's functions, the analytical theory is established in Sec. III. Section IV presents the theoretical analysis results which are well agreed with that obtained by computer simulation, and the various situations of the excitation by line charge of electron beams with different energy and different thickness of the holes. In Sec. V, the distinct differences between the phenomenon excited by a line charge of electron beam and a plane wave are compared and discussed. Finally, Sec. VI is the conclusion.

II. COMPUTER SIMULATION

The model concerned is with the geometry shown in Fig. 1. The contour maps obtained by means of computer simulation (PIC codes) are given in Fig. 2. It shows that a line charge moving parallel to the array on one side excites the diffraction radiation on both sides of the SHA with the same diffraction radiation angle, minor amplitude decay and no phase delay. It should be emphasized the fact that there is no phase delay between the diffraction radiation waves on the both sides of the SHA in such simulation case shown in Fig. 2. Figures 2(a) and 2(b) show that in the SHA each hole radiates individually as a radiation cell, and in a cell each point serves the original radiation sources. All these cells get

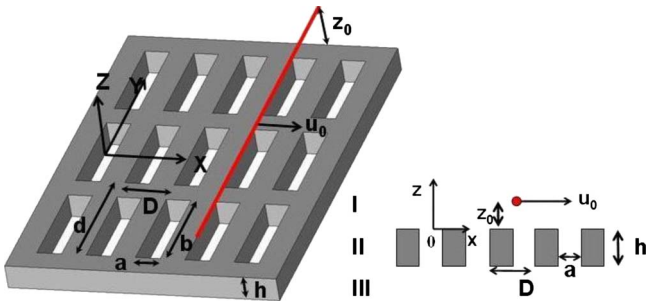

FIG. 1. (Color online) Schematic structure of holes array considered in the work: a holes array of rectangular holes in a perfect metal of thickness h. The period in x direction is D and is in y direction d, while the sides of hole are $a=0.5D$, $b=2D$, $D=0.6$ mm. The distance between the line charge (with velocity u_0) and the upper surface of the structure is z_0. The model can be divided into three regions: the upper half space (region I), the lower half space (region III) and the holes array (region II).

*hu_m@uestc.edu.cn

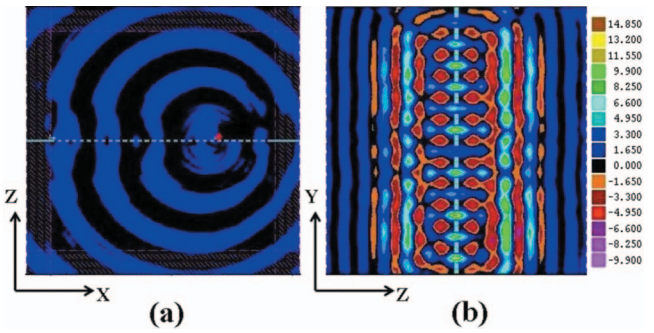

FIG. 2. (Color) Computer simulation of the diffraction radiation from SHA. The energy of line charge is 10 kV, and the thickness of SHA is $0.2D$. (a) Simulation result of contour map of B_z on x y plane in a SHA. The red point represents the unit line charge. (b) Simulation result of contour map of B_z on y z plane at the 10th period length in x direction of a SHA.

together to organize the entire diffraction radiation to form a diffraction radiation array. These physical processes reflect an exceptional case of Huygen's principle. The diffraction radiation shown in Fig. 2 inhibits the distinct radiation characteristics and processes from others [23–25]. The above results indicate that under the excitation of the line charge, a SHA becomes a diffraction radiation array, a distinct diffraction radiation mechanism is discovered.

Figures 3(a)–3(c) show the simulation results of fields in the fixed points in both the upper and lower half spaces with the same distance (8 periods) far away from each surface of the SHA. The energy of line charge is 10 kV, and the thickness of SHA is $0.2D$. Figure 3(a) shows the fact that the radiation fields in the both half spaces diffracted from each side of the structure are with the same phase indicates obviously that the diffraction radiation waves in both the lower half space and the upper half space are excited at the same time. This fact leads to the conclusion that the wave fields are passing through the holes without any time delay under this simulation situation. The theoretical analysis and calculations given in the next two sections of the paper will indicate that the properties of the fields passing through the holes array are different for different beam energies.

III. THEORY

Based on the mathematical formulation of Huygens's principle, the analytical theory can be established to describe the entire above phenomena. But before doing this, it is necessary to make these simulated phenomena surely clear.

A. Physical processes

Passing parallel to the surface of the SHA, line charge of electron beam excites a set of evanescent waves. Part of these waves is propagating along the array as mimicking surface plasmon modes, and part of them is transformed to be diffraction radiation wave taking the energy away in the upper space. The rest part passes through the holes into another side of the array and induces the similar physical pro-

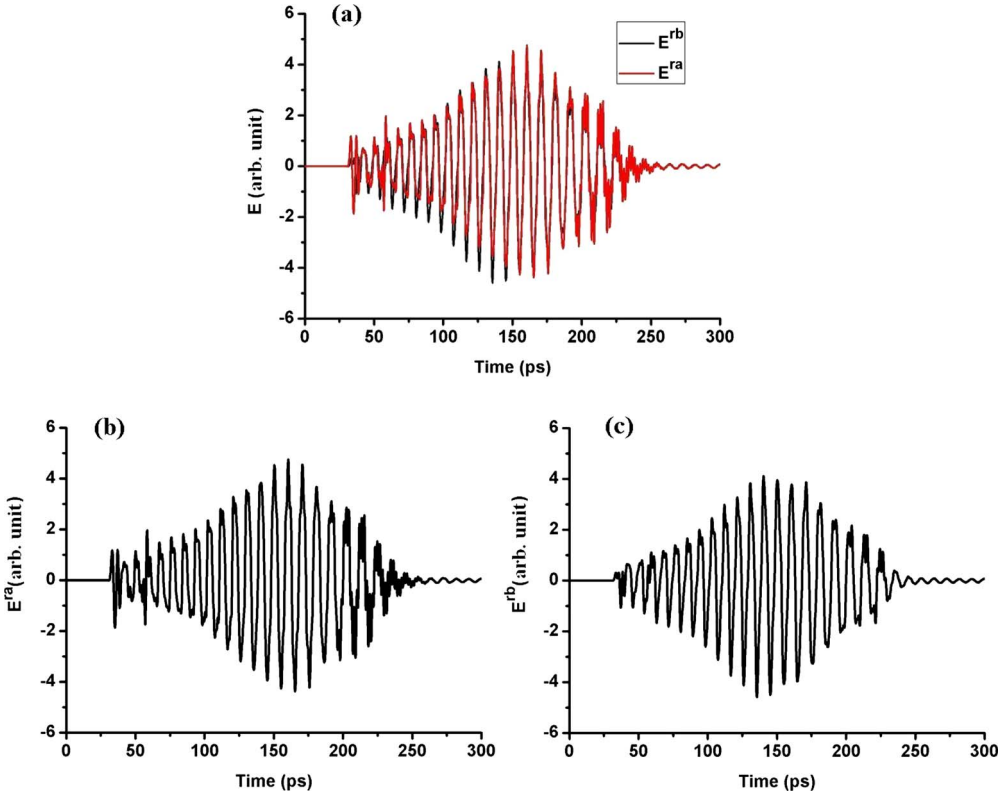

FIG. 3. (Color online) Radiation fields. (a) Simulation result of radiation E^{ra} and E^{rb}; (b) simulation result of radiation field E^{ra} in the upper half space; (c) simulation result of radiation field E^{rb} in the lower half space. It shows that components of the fields with the same frequency are in the same phases on both sides, respectively.

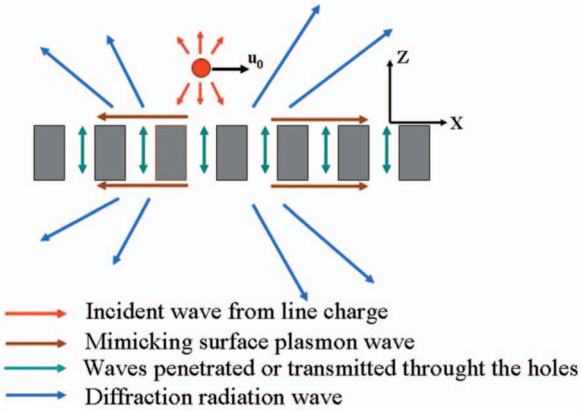

FIG. 4. (Color) Physical processes.

cesses in the lower half space. All these phenomena are shown in Fig. 4. The most important and interesting point is that all these physical processes happen simultaneously for lower beam energy and thin thickness of this array as shown in Figs. 2 and 3.

At first, the dispersion relation of the mimicking surface plasmon waves propagating along the surface of the SHA should be developed. The eigenvalue approach of the Maxwell's equations together with boundary conditions gives the dispersion equation. There are many modes in the holes but only the fundamental mode TE_{01} is focused because it is the easiest mode to be excited in the holes. The dispersion equation is obtained and the derivation is given in Appendix A

$$\frac{k_{zh}}{k_0^2}\frac{1+e^{-jk_{zh}h}}{1-e^{-jk_{zh}h}} = \frac{a}{D}\sum_{m=-\infty}^{\infty} \mathrm{sinc}^2\left(\frac{k_{xm}a}{2}\right)\frac{1}{k_{zm}} \tag{1}$$

where $k_{xm}=k_x+2m\pi/D$ is the wave vector in x direction of region I, $k_{zm}=\sqrt{k_0^2-k_{xm}^2}$ is the wave vector in z direction of region I shown in Fig. 1 and $k_{zh}=\sqrt{k_0^2-(\pi/b)^2}$ is the wave propagation vector in the small waveguide (hole).

The line charge of electron beam with a fixed velocity induces a set of evanescent waves which contain plenty of frequency components. According to the Bloch-Floquet theorem, these waves should be expanded into infinite space harmonics to match the boundary condition shown in Fig. 1. The space harmonics falling into the gray domain bounded by the positive and negative light lines shown in Fig. 5 can radiate from the surface of the SHA. Figure 5 shows that only the negative space harmonics can be the radiative waves in a definite frequency region determined by the velocity of the line charge. For the case of electron beam energy is 10 kV, $D=0.6$ mm, the first negative harmonic ($n=-1$) can radiate in the frequency region from P1 point to P2 which is just below the cut-off frequency of the holes, while the second negative harmonic radiate in the frequency region from P3 point to P4, the frequency of which is twice higher than that of the first negative harmonic. It can be seen that the first negative harmonic carries the most part of the energy of the radiative waves. It means that simulation results of the frequency and amplitude of the diffraction field in the upper half space mainly depend on the first negative harmonic.

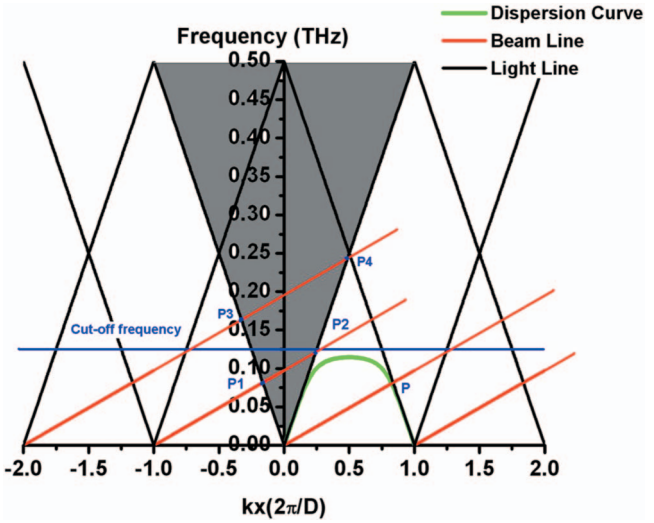

FIG. 5. (Color) Dispersion Brillouin diagram: the green line is the calculated dispersion curve in the fundamental space harmonic, the cross of the red beam line with beam energy 10 kV and the dispersion curve is the work point P which is below the cut-off frequency (the blue line) of holes.

According to the Brillouin diagram shown in Fig. 5, the diffraction frequency of the first negative harmonic is lower than the cut-off frequency of the holes, it indicates that the most energy of the diffraction radiation wave cannot transmit through but can penetrate into [26] the holes array without phase delay.

As mentioned above that a set of evanescent waves induced by a line charge are propagating along the surface of the array, and these waves should be expanded into space harmonics to meet the boundary conditions. Some of these space harmonics propagate along the surface of the SHA as mimicking surface plasmon waves, while a part of them is diffracted to the upper half space taking the energy away. As shown in Fig. 5 all of the space harmonics of the rest part of the waves can penetrate through the holes of the array and reach the open exist of the holes in the back side of the array. And then similar set of evanescent waves and their space harmonics with minor amplitude decay excited as the surface waves propagate along the surface of the back side of the SHA, and hence the diffraction radiation occurs in the lower half space just like that happens in the upper half space shown in Fig. 5. It should be emphasized in this case that all the above physical processes as a whole happen simultaneously.

B. Analytical theory

Making use of the integral equations together with the relevant Green's functions, the analytical theory for such a complicated system has been established [27]. The proper Green's functions of these regions should be found and applied in the integral equations to solve the diffraction and penetration fields separately. Finally, the boundary conditions are matched to determine the coefficients of the wave fields.

The original wave fields can be found by solving the Helmholtz equation which is given in Appendix B in detail.

The frequency components of E_x^i can be obtained

$$E_x^i(\omega) = \frac{qk_x}{2\epsilon_0 u_0 k_z}(1-\beta^2)e^{jk_x x}e^{-k_z^i|z-z_0|}, \tag{2}$$

where q is the charge, u_0 is the velocity of the line charge and $k_x=\omega/u_0$, $k_z=\sqrt{k_0^2-k_x^2}=j\sqrt{k_x^2-k_0^2}=jk_z^i$, $\beta=u_0/c$.

All other field components can be found in terms of E_x by means of Maxwell's equations.

Making use of the following integral equation, the diffraction radiation field E_x^d in upper and lower half spaces and the field in the holes E_x^h can be found

$$E_x^{d,h}(x,y,z;\omega) = \int\int_s (G\nabla E_x^{d,h} - E_x^{d,h}\nabla G)\cdot dS, \tag{3}$$

where $G=G(x,y,z;x',y',z')$ is the required Green's function, and ∇G, $\nabla E_x^{d,h}$ are the gradient of the Green's function and the electric field in the outer normal direction of the integral surface, respectively.

Now the following three Green's functions [28,29] for the upper half space, the holes and the lower half space have been found for the integral equations of the diffraction radiation on both sides and the wave in holes

$$G^{ra} = \sum_{m=-\infty}^{\infty}\sum_{n=-\infty}^{\infty}\frac{jabQ}{2k_{zmn}dD}\mathrm{sinc}\left(\frac{k_{xm}a}{2}\right)e^{jk_{xm}(x-x')}e^{jk_{zmn}(z-z')} \times\cos\left(\frac{2n\pi}{d}y\right)\cos\left(\frac{2n\pi}{d}y'\right), \tag{4}$$

$$G^h = \sum_{p=0}^{\infty}\sum_{q=0}^{\infty}\frac{2j}{abk_{zpq}}\cos\left(\frac{p\pi}{a}x\right)\cos\left(\frac{p\pi}{a}x'\right)\cos\left(\frac{q\pi}{b}y\right) \times\cos\left(\frac{q\pi}{b}y'\right)(e^{jk_{zpq}(z-z')}+e^{-jk_{zpq}(z-z')}), \tag{5}$$

$$G^{rb} = \sum_{m=-\infty}^{\infty}\sum_{n=-\infty}^{\infty}\frac{jabQ}{2k_{zmn}dD}\mathrm{sinc}\left(\frac{k_{xm}a}{2}\right)e^{jk_{xm}(x-x')}e^{jk_{zmn}(z-z')} \times\cos\left(\frac{2n\pi}{d}y\right)\cos\left(\frac{2n\pi}{d}y'\right). \tag{6}$$

Where G^{ra}, G^{rb}, and G^h are the relevant Green's function for upper and lower half spaces and the holes, respectively. In Eqs. (4) and (6), m and n denote the space harmonics, and in Eq. (5) p and q are the mode number of all of the modes in the hole. G^h represents the Green's function in the holes considering the full expansion on waveguide modes. The mathematical manipulation of these Green's functions are given in Appendix C.

At first the study is for the case of infinitely thin holes, $h\to 0$. For this case, the Green's function for the holes Eq. (5) is not needed. Substituting Eqs. (4) and (6) into the integral equation Eq. (3), the following diffraction radiation in both sides of the thin film array can be obtained

$$E^{ra} = \sum_m\sum_n A_{mn}e^{jk_{xm}x}e^{jk_{zmn}|z|}\cos\left(\frac{2n\pi y}{d}\right), \tag{7}$$

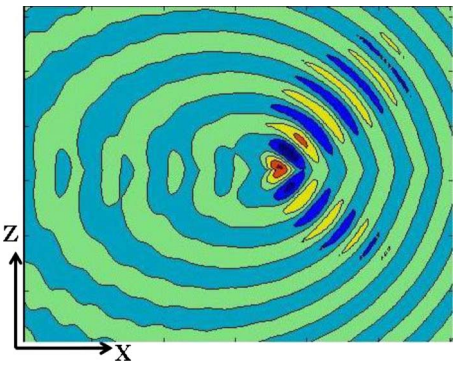

FIG. 6. (Color online) Calculated filed contour for the case beam energy is 10 kV, $h=0.2D$.

$$E^{rb} = \sum_m\sum_n A_{mn}e^{jk_{xm}x}e^{-jk_{zmn}|z|}\cos\left(\frac{2n\pi y}{d}\right). \tag{8}$$

The difference between Eqs. (7) and (8) is only the factor $e^{jk_{zmn}|z|}$ for upper half space ($z>0$) and $e^{-jk_{zmn}|z|}$ for lower half space ($z<0$). Figures 2, 6, and 10 apparently show that the diffraction radiation is on both sides of the array. The similar symmetry of fields is also proven in Ref. [30] [p. 636, Eq. (1)].

The frequency-angle dependence of the diffraction radiation can also be easily achieved. From Helmholtz equation, the following relation holds

$$k_{xm}^2 + k_{zm}^2 = k_0^2 = \left(\frac{\omega}{c}\right)^2, \tag{9}$$

$$k_{xm} = \frac{\omega}{u_0} + \frac{2m\pi}{D} = k_0\cos(\theta), \tag{10}$$

where c is the speed of light in vacuum and θ is the diffraction radiation angle. Then, the relation of the wavelength λ and radiation angle θ can be obtained

$$\lambda = -\frac{D}{m}\left(\frac{1}{\beta}-\cos(\theta)\right). \tag{11}$$

It is just that of Smith-Purcell radiation. Equations (9) and (11) show that this frequency-angle dependence of the radiation is the natural result of the Maxwell's equation. It shows that generally the Smith-Purcell radiation is diffracted into both sides of a periodical system with the same angle dependence of the radiation rather than only in upper half space.

Now it is the time to study the diffraction radiation of the model shown in Fig. 1 where the thickness of the hole is with finite value. The problem becomes much complicated for that before diffracting in the lower half space, the waves should pass through the holes either by transmission or by penetration. Therefore, all the three Green's functions Eqs. (4)–(6) are needed.

Substituting the relevant Green's functions into Eq. (3), the diffraction radiation fields in upper and lower half spaces E^{ra}, E^{rb}, and the penetration or transmission wave fields in

the holes E^h can be obtained, respectively, while the use of the orthogonality relations of different space harmonics and different waveguide modes are made.

For the simplicity without sacrificing the generality, only the lowest mode in the small waveguide (hole), the TE_{01} mode which is the most easiest excited mode is considered [7]. Solving the integration equation, the wave fields in three regions can be obtained

$$E^{ra} = \sum_m \sum_n B_{1mn} e^{jk_{xm}x} e^{jk_{zmn}z} \cos\left(\frac{2n\pi}{d} y\right), \tag{12}$$

$$E^h = (B_2 e^{jk_{zh}z} + B_3 e^{-jk_{zh}z}) \cos\left(\frac{\pi}{b} y\right), \tag{13}$$

$$E^{rb} = \sum_m \sum_n B_{4mn} e^{jk_{xm}x} e^{jk_{zmn}z} \cos\left(\frac{2n\pi}{d} y\right). \tag{14}$$

The coefficients B_{1mn}, B_2, B_3, and B_{4mn} are determined by matching the boundary conditions at $z=0$ and $z=-h$. It should be noticed that in Eq. (13) the multiple reflection processes finally can be replaced by the coefficients B_2 and B_3. The detailed derivation is present in Appendix D.

IV. NUMERICAL CALCULATION RESULTS

A. Calculation results for beam energy 10 kV and thickness 0.2*D*

In the case of beam energy 10 kV and the thickness 0.2*D*, the radiation frequency of the first negative harmonic is in the cut-off frequency region shown in Fig. 5. Figure 6 shows the calculated field contour map based on the theory for this case. It can be seen that the calculated contour map is in consistent with that simulated by computer simulation shown in Fig. 2(a). Figure 6 also confirms the electromagnetic penetration of the subwavelength holes. It can be seen from Eq. (13) that the propagating factors of field in the hole $B_2 e^{jk_{zh}z}$ and $B_3 e^{-jk_{zh}z}$ are considered. In this case, the field frequency is below the cut-off frequency of the hole, hence the wave vector k_{zh} is imaginary, and the propagating factor becomes an attenuation factor, so there is no phase change, instead, there is only amplitude decay.

Figures 7(a) and 7(b) show the simulated and calculated diffraction radiation field at a definite point in the lower half spaces of the SHA. The line charge is moving from the left to the right, so the radiation angle is changing from 0 to π. The diffraction radiation frequencies at the fixed point are time dependent ranging from 0.089 to 0.119 THz shown in Fig. 7(a), and that for the calculated ranging from 0.086 to 0.121 THz is shown in Fig. 7(b). The discrepancy of the maximum and minimum frequencies is due to the initial condition of the calculation. The model of the theory is assumed infinite long in x and y direction, but that used in the computer simulation is only 25*20.

The frequencies of field E^h of simulated result in the center of the holes and that of the calculated results based on the theory are the same. It equals to 0.1 THz and is agreed with the work point P on the dispersion curve shown in Fig. 5.

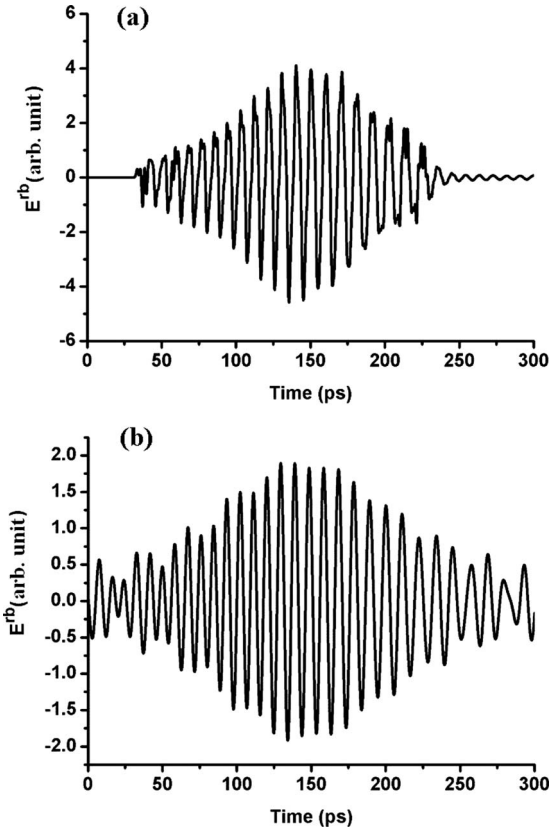

FIG. 7. Radiation fields. (a) Simulation result of radiation fields E^{rb} in the lower half space. (b) Calculated field E^{rb} in the lower half space.

Therefore, Figs. 6 and 7 show that all these calculated results are well agreed with that of the simulation result from computer simulation. It should be emphasized that in this case all the physical processes including the diffraction radiation on the both sides of the array and the electromagnetic penetration through the holes of the array happen simultaneously.

B. The dependence of beam energy and the influence of the holes thickness

This paper mainly explores the SHA diffraction radiation. However, the electromagnetic penetration or transmission could not be avoided for they are accompanied by the diffraction radiation. Here, only those penetration or transmission problems which are closely connected with the diffraction radiation are studied.

It should be noticed that from the dispersion Brillouin diagram the diffraction radiation frequency and electromagnetic penetration or transmission depend on the beam energy and the thickness of the holes. Increasing the energy of the line charge, the diffraction radiation frequency region of the first negative harmonic is increased also, and in general it carries the most part of the diffraction radiation wave. Adjusting the voltage of the line charge to 15 kV shown in Fig. 8(a), the diffraction radiation frequency region of the first space harmonics is from S1 to S3 and crosses the cut-off

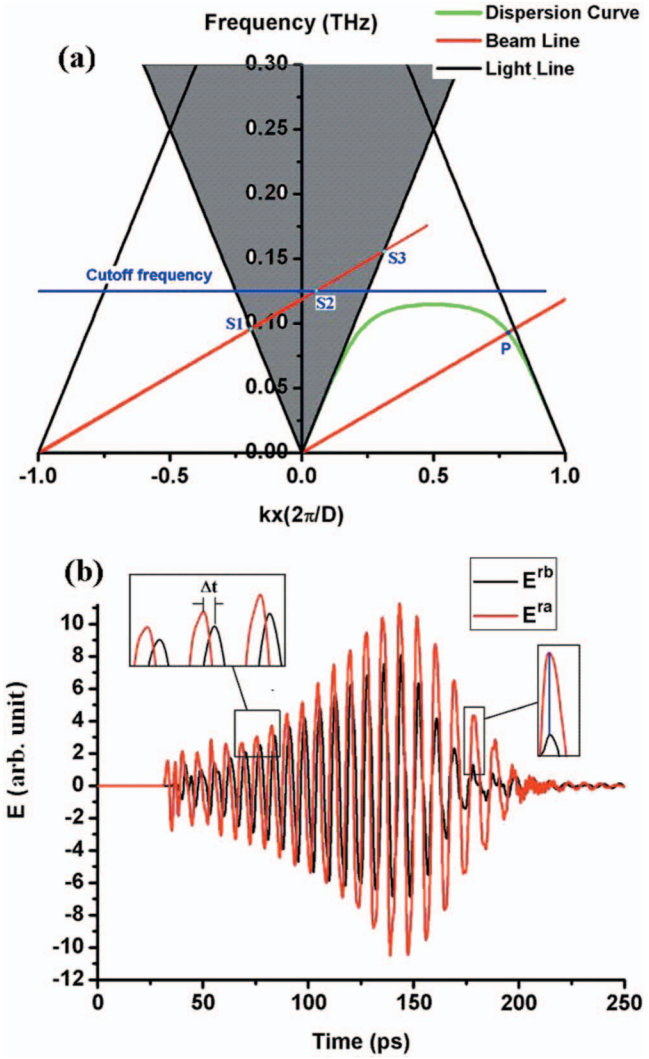

FIG. 8. (Color) Radiation fields. (a) Dispersion Brillouin diagram for 15 kV line charge of electron beam, $h=2D$. (b) Simulation result of diffraction radiation fields in both sides of the SHA. Since the frequency in the region that is higher than the cut-off frequency, there is phase delay in the frequency region from S2 to S3.

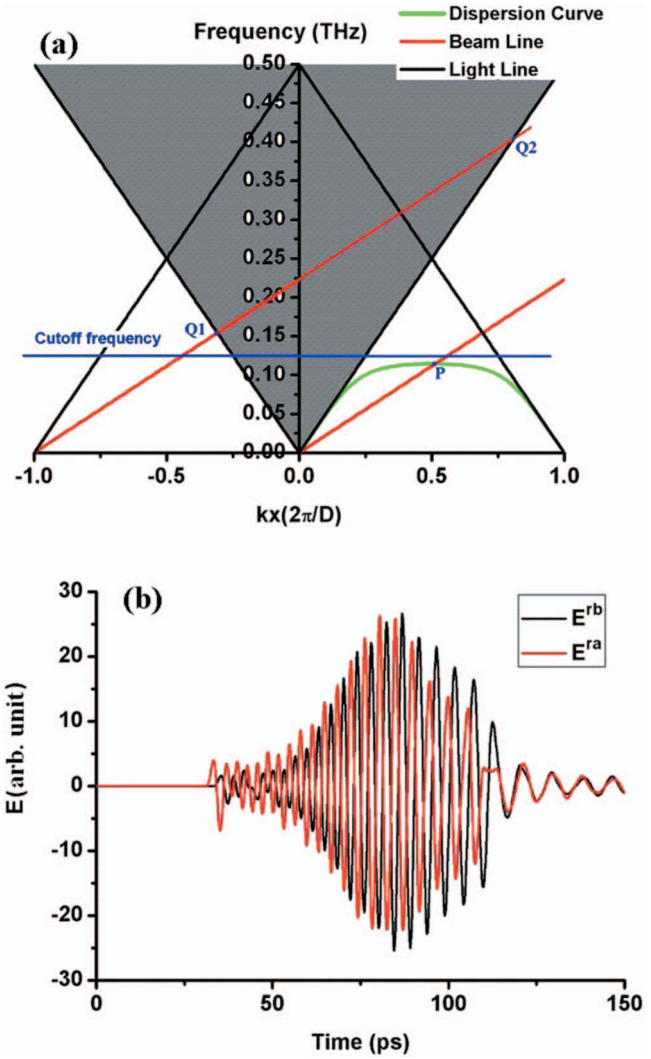

FIG. 9. (Color) Radiation fields. (a) Dispersion Brillouin diagram for 60 kV line charge of electron beam, $h=2D$. (b) Simulation result of diffraction radiation fields in both sides of the SHA. It shows that there is phase delay.

frequency at point S2. It means that part of the diffraction radiation wave in the region between S2 to S3 can transmit through the holes with phase delay and that from S1 to S2 should penetrate into the holes without phase delay. This fact is confirmed by comparing the phases of the two side diffraction radiation shown in Fig. 8(b).

Further increasing the beam energy up to 60 kV, it happens that the frequency regions of all the diffraction radiation space harmonics are higher than the cut-off frequency as shown in Fig. 9. In this case, the frequency region of the first negative harmonic located from Q1 to Q2 shown in Fig. 9(a). As shown in Fig. 9(b), now the diffraction radiation waves between the upper and lower side of SHA has a phase delay obviously. This phenomenon is also confirmed by the simulated and calculated contour maps shown in Fig. 10.

The studies on the various cases with different beam energy and different thickness of the holes surely confirm the validity of the model and the theory for the discovered diffraction radiation array.

V. DISCUSSION

As mentioned above, a large number of published papers are devoted to the transmission and reflection of the SHA excited by a plane waves. Therefore, it is interesting to discuss the differences of the whole phenomenon excited by a line charge of electron beam and that by a plane wave. In the case of the electron beam excitation, the original wave is a set of evanescent wave, which contains plenty of frequency components; while in the plane wave case, the incident wave is a coherent wave with a fixed frequency. In the both cases, the mimicking surface plasmon waves consist of the space harmonics. It has been proven that in the first case, the frequency of diffraction radiation on a fixed point of either side is changeable depending upon the radiation angle, which is determined by the distance from the line charge to the observed point and the velocity of the moving line charge. But in the plane wave excitation case, the incident plane wave and all harmonics are the waves with only one fixed fre-

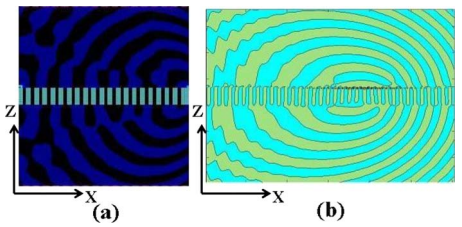

FIG. 10. (Color online) Contour maps. (a) Simulation result of contour map for 60 kV line charge of electron beam, $h=2D$. (b) Calculated contour map for 60 kV line charge of electron beam, $h=2D$. The contours show that there are phase delay of the diffraction between the two sides.

quency independent of the incident angle. Besides, in the electron beam excitation case, the frequency of the penetration wave depends only on the size of the holes and the speed of the line charge, while in the plane wave case, the frequency of the penetration is also the same with the incident plane waves. And it is obvious that the classical integration equation approach can also be used in the case of plane wave.

In the Refs. [20,21], the mimicking surface plasmon transmission and super-radiant radiation through the rectangular holes array excited by two electron beams moving in opposite directions have been studied. But the theoretical analysis [22] for the papers [20,21] is for metal slits in which the fundamental electromagnetic mode is TEM mode that has no cut-off frequency and cannot exist in the rectangular hole. Also, the diffraction radiation companied with the electromagnetic transmission is not considered.

VI. CONCLUSION

In conclusion, under the excitation by a set of evanescent waves generated by the line charge of electron beam, a distinct mechanism of the three dimensional diffraction radiation is discovered and the electromagnetic penetration or transmission through SHA is confirmed. The calculated results of the analytical theory are well agreed with that obtained by computer simulation. The following points revealed in this paper are of great significance in physics and optics:

(1) The diffraction radiation induced by moving charge is on both sides of the array with the same frequency-angle relation. It is the extension of the Smith-Purcell radiation. However, when the thickness of the holes is with finite value, the physical processes become much complicated.

(2) The diffraction radiation waves on both sides of the SHA may have different behaviors depending on the velocity of the line charge and the thickness of the holes. In case of low energy and thin thickness, the two side diffraction radiation are excited simultaneously with the same diffracted angle and minor amplitude decay. In case of higher beam energy and large thickness, the diffraction radiation waves in the lower half space may have phase delay. But in all these cases, the diffraction radiation angle in both sides of the array is the same.

(3) The duration of the line charge passing through the whole structure is just in picoseconds. Therefore, for a chain of the line charge excitation, a chain of the ultrashort diffraction radiation with fine inner structure should occur which is a wonderful physical phenomenon. It may have potential applications in THz science and technology.

This discovery is of great significant for physics and optics. It is also important for practical applications, in particular for the THz radiation sources and devices. Moreover, the integral equations method for the analytical theory of the diffraction radiation and the electromagnetic penetration/transmission of the SHA can also be extended to explore other interesting phenomena with SHA structure.

ACKNOWLEDGMENTS

The authors would like to acknowledge Dr. Peter H. Siegel of the California Institute of Technology, USA for his interest and support of this work. This work is supported by National Key Programme of Fundamental Research of China under Contract No. 2007CB310401, and National Natural Science Foundation of China under Contract No. 60472013.

APPENDIX A: DISPERSION RELATION

In this appendix, the dispersion relation is derived. Using Floquet theory, the field components of E_x and H_y in the region I are described as follows

$$E_x^I = \sum_{m=-\infty}^{\infty} C_m e^{jk_{zm}z} e^{jk_{xm}x}, \tag{A1}$$

$$H_y^I = \sum_{m=-\infty}^{\infty} \frac{\omega\epsilon_0}{k_{zm}} C_m e^{jk_{zm}z} e^{jk_{xm}x}, \tag{A2}$$

where $k_{xm}=\omega/u_0+2m\pi/D$, $k_{zm}^2=k_0^2-k_{xm}^2$. Here, the wave factor $e^{-j\omega t+jk_{xm}x+jk_{zm}z}$ is used, and $e^{-j\omega t}$ is ignored in the paper.

In region II, only the fundamental mode TE_{01} are considered as

$$E_x^{II} = (Ae^{jk_{zh}z} + Be^{-jk_{zh}z})\cos\left(\frac{\pi y}{b}\right), \tag{A3}$$

$$H_y^{II} = \frac{k_{zh}}{\omega\mu_0}(Ae^{jk_{zh}z} - Be^{-jk_{zh}z})\cos\left(\frac{\pi y}{b}\right), \tag{A4}$$

where $k_{zh}=\sqrt{k_0^2-(\pi/b)^2}$ is the wave propagation vector in the hole.

Then, the following boundary conditions should be satisfied. It should be noticed that the boundary condition matching can be enforced over one periodical cell. The E_x field component must be continuous over the whole surface of one period, and the H_y field component must be continuous just over the hole. This approach is often used [5].

The boundary condition at $z=0$

$$E_x^I(z=0) = E_x^{II}(z=0),$$

$$\frac{1}{D}\int_{-D/2}^{D/2} H_y^I(z=0)dx = H_y^{II}(z=0).$$

Considering the symmetrical structure in z direction, another boundary condition at $z=-h/2$ is

$$H_y^{II}(z=-h/2)=0$$

The dispersion relation of the model can be expressed as

$$\frac{k_{zh}}{k_0^2}\frac{1+e^{-jk_{zh}h}}{1-e^{-jk_{zh}h}}=\frac{a}{D}\sum_{m=-\infty}^{\infty}\mathrm{sinc}^2\left(\frac{k_{xm}a}{2}\right)\frac{1}{k_{zmn}}. \tag{A5}$$

APPENDIX B: ORIGINAL WAVE FIELDS

The vector and scalar potentials A and φ are involved and the Maxwell's equations are rewritten as

$$\nabla^2\varphi-\epsilon_0\mu_0\frac{\partial^2\varphi}{\partial t^2}=-\frac{\rho}{\epsilon}, \tag{B1}$$

$$\nabla^2 A-\epsilon_0\mu_0\frac{\partial^2 A}{\partial t^2}=-\mu J, \tag{B2}$$

$$E=-\nabla\varphi-\frac{\partial A}{\partial t} \tag{B3}$$

$$B=\nabla\times A. \tag{B4}$$

The Lorenz gauge is used

$$\nabla\cdot A+\epsilon\mu\frac{\partial\varphi}{\partial t}=0. \tag{B5}$$

The electron charge density and the line charge density are

$$\rho=q\delta(x-u_0t)\delta(z-z_0), \tag{B6}$$

$$J_x=qu_0\delta(x-u_0t)\delta(z-z_0), \tag{B7}$$

where q is the charge, u_0 is the speed of the line charge and $k_x=\omega/u_0$, $k_z^i=\sqrt{k_x^2-k_0^2}$.

Writing the electric charge density and transforming it to Fourier integral, we get

$$\rho=q\delta(x-u_0t)\delta(z-z_0)=\frac{q}{4\pi^2}\int\int e^{jk_x(x-u_0t)}e^{jk_z(z-z_0)}dk_xdk_z. \tag{B8}$$

Substituting the Eq. (B8) into Eq. (B1) and involving with the residue theory and keeping only one of the two residues, the frequency components of the solution of φ can be obtained

$$\begin{aligned}\varphi(t)&=\frac{q}{4\pi^2\epsilon_0}\int\int\frac{e^{jk_x(x-u_0t)+jk_z(z-z_0)}}{k_z^2+k_x^2-k_0^2}dk_xdk_z\\&=\frac{jq}{4\pi\epsilon_0}\int\frac{e^{jk_x(x-u_0t)+jk_z(z-z_0)}}{k_z}dk_x\\&=\frac{1}{2\pi}\int\frac{jq}{2\epsilon_0u_0}\frac{e^{jk_xx+jk_z(z-z_0)}}{k_z}e^{-j\omega t}d\omega,\end{aligned} \tag{B9}$$

$$\varphi(\omega)=\frac{jq}{2\epsilon_0u_0k_z}e^{jk_xx+jk_z|z-z_0|}. \tag{B10}$$

And the vector potential is

$$A_x(\omega)=\epsilon\mu u_0\varphi(\omega)=\frac{jq\mu_0}{2k_z}e^{jk_xx+jk_z|z-z_0|}, \tag{B11}$$

where $k_x=\omega/u_0$, $k_z^2=k_0^2-k_x^2$ and $\beta=u_0/c$. Since $u_0<c$, k_z is an imaginary value, we define $k_z^i=\sqrt{k_x^2-k_0^2}$.

Then, the solution of electric field E_x^i can be obtained

$$\begin{aligned}E_x^i(\omega)&=-\nabla\varphi-\frac{\partial A}{\partial t}\\&=-jw\left[\frac{\nabla(\nabla\cdot A)}{k_0^2}-A\right]\\&=\left(\frac{qk_x}{2\epsilon_0u_0k_z}-\frac{q\omega\mu_0}{2k_z}\right)e^{jk_xx}e^{-k_z^i|z-z_0|}\\&=\frac{qk_x}{2\epsilon_0u_0k_z}(1-\beta^2)e^{jk_xx}e^{-k_z^i|z-z_0|}.\end{aligned} \tag{B12}$$

APPENDIX C: GREEN'S FUNCTIONS

In this appendix we present determination of the Green's functions in three different regions. The Green's functions in both half spaces introduced in Sec. III satisfy the following Helmholtz equation

$$\nabla^2G^{ra,rb}+k_0^2G^{ra,rb}=-\delta(x-x')\delta(z-z'),$$

$$\partial^2G/\partial x^2+\partial^2G/\partial z^2+k_0^2G=-\delta(x-x')\delta(z-z'). \tag{C1}$$

The Green's functions should be the solution of Eq. (C1) and also fulfill the boundary conditions at $z=0$ for the upper half space and $z=-h$ for the lower half space. Both of them are two half space Green's functions in z direction, and are determined only by the field distribution in x direction and y direction. Due to the symmetry of the structure in z direction, the Green's function in upper and lower half space G^{ra} and G^{rb} are the same.

It can be expanded by Floquet's theorem with period D in x direction

$$G(x,z;x',z')=\sum_{m=-\infty}^{\infty}g_m(z;z')e^{jk_{xm}(x-x')}. \tag{C2}$$

Substituting Eq. (C2) into Eq. (C1)

$$\begin{aligned}&\sum_{m=-\infty}^{\infty}[\partial^2g_m/\partial z^2+(k_0^2-k_{xm}^2)g_m]e^{jk_{xm}(x-x')}\\&\quad=-\delta(x-x')\delta(z-z').\end{aligned} \tag{C3}$$

Multiplying by $e^{jk_{xm}x'}$ in both sides, integrating in a period in x direction and using the orthogonality of $e^{jk_{xm}x'}$, it can be obtained

$$\partial^2 g_m/\partial z^2 + (k_0^2 - k_{xm}^2) g_m = -\delta(z-z')A_m, \tag{C4}$$

where A_m is the coefficient and can be determined by the boundary condition in x direction. The solution of Eq. (C4) is [28]

$$g_m = \frac{-A_m}{2\pi}\int \frac{e^{jk_{zmn}(z-z')}}{-k_{zmn}^2 + k_0^2 - k_{xm}^2} dk_{zmn} = A_m \frac{j}{2k_{zmn}} e^{jk_{zmn}(z-z')}, \tag{C5}$$

where $k_{xm}=k_x+\frac{2m\pi}{D}$, $k_{zmn}^2=k_0^2-k_{xm}^2-k_{yn}^2$, $k_{yn}=0$.

Only the TE_{01} mode is considered in the paper, so the electric field is a constant value in the exit of the hole with width a $(a<D)$ periodically in x direction

$$A_m = \frac{1}{D}\int_{-D/2}^{D/2} e^{jk_{xm}x} dx = \frac{1}{D}\int_{-a/2}^{a/2} e^{jk_{xm}x} dx = \frac{a}{D}\mathrm{sinc}\left(\frac{k_{xm}a}{2}\right). \tag{C6}$$

Substituting Eqs. (C5) and (C6) into Eq. (C2), the Green's function can be derived as

$$G = \sum_{m=-\infty}^{\infty} \frac{ja}{2Dk_{zmn}} \mathrm{sinc}\left(\frac{k_{xm}a}{2}\right) e^{jk_{xm}(x-x')} e^{jk_{zmn}(z-z')}.$$

The distribution of electric field on the surface of the array is $\cos(\frac{\pi}{b}y)(b<d)$ periodically in y direction, hence the Fourier series approach should be used to expand the Green's function with $\cos(\frac{2n\pi}{d}y)\cos(\frac{2n\pi}{d}y')$ form to match the boundary. For the constant term of the expansion with $n=0$ should be avoid, only the positive mode index n are considered. Then the Green's functions for both upper and lower half spaces can be obtained

$$G^{ra,rb} = \sum_{m=-\infty}^{\infty}\sum_{n=1}^{\infty} A_m B_n \frac{j}{2k_{zmn}} e^{jk_{xm}(x-x')} e^{jk_{zmn}(z-z')} \times \cos\left(\frac{2n\pi}{d}y\right)\cos\left(\frac{2n\pi}{d}y'\right). \tag{C7}$$

The coefficient B_n is determined by the boundary conditions in y direction

$$B_n = \frac{1}{d}\int_{-b/2}^{b/2} \cos\left(\frac{\pi}{b}y\right)\cos\left(\frac{2n\pi}{d}y\right)dy = \frac{b}{d}\left[\mathrm{sinc}\left(\frac{\pi}{2}+\frac{bn\pi}{d}\right) + \mathrm{sinc}\left(\frac{\pi}{2}-\frac{bn\pi}{d}\right)\right]. \tag{C8}$$

We define $Q=\mathrm{sinc}(\frac{\pi}{2}+\frac{bn\pi}{d})+\mathrm{sinc}(\frac{\pi}{2}-\frac{bn\pi}{d})$.

Then, Green' functions are obtained as

$$G^{ra,rb} = \sum_m\sum_n \frac{jabQ}{2k_{zmn}dD}\mathrm{sinc}\left(\frac{k_{xm}a}{2}\right) e^{jk_{xm}(x-x')} e^{jk_{zmn}(z-z')} \times \cos\left(\frac{2n\pi}{d}y\right)\cos\left(\frac{2n\pi}{d}y'\right). \tag{C9}$$

The Green's function in the hole region can be derived by the same way. For a rectangular hole, the Green's function can be solved from the following Helmholtz equation

$$\nabla^2 G^h + k_0^2 G^h = -\delta(x-x')\delta(y-y')\delta(z-z'). \tag{C10}$$

The boundary conditions are: $G=0$ at $x=-a/2$, $x=a/2$, $y=-b/2$, and $y=b/2$, so the Green's function can be expanded into a Fourier series in both x and y direction

$$G^h = \sum_{p=0}^{\infty}\sum_{q=0}^{\infty} g_{pq}(z;z')\cos\left(\frac{p\pi}{a}x\right)\cos\left(\frac{q\pi}{b}y\right). \tag{C11}$$

Substituting Eq. (C11) into Eq. (C10) and multiplying by $\cos(\frac{p\pi}{a}x)$ and $\cos(\frac{q\pi}{b}y)$ in both sides, integrating from $x=-a/2$ to $x=a/2$ in x direction and integrating from $y=-b/2$ to $y=b/2$ in y direction, and according to the orthogonality of trigonometric functions, it can be obtained

$$\left[\frac{\partial^2}{\partial z^2} - \left(\frac{p\pi}{a}\right)^2 - \left(\frac{q\pi}{b}\right)^2 + k_0^2\right] g_{pq} = -\delta(z-z')\frac{4}{ab}\cos\left(\frac{p\pi}{a}x'\right)\cos\left(\frac{q\pi}{b}y'\right). \tag{C12}$$

The solution of Eq. (C12) is [28]

$$g_{pq} = \frac{-4}{ab}\cos\left(\frac{p\pi}{a}x'\right)\cos\left(\frac{q\pi}{b}y'\right)\frac{1}{2\pi} \times \int \frac{e^{jk_{zpq}(z-z')}}{-k_{zpq}^2 - \left(\frac{p\pi}{a}\right)^2 - \left(\frac{q\pi}{b}\right)^2 + k_0^2} dk_{zpq} = \frac{2j}{abk_{zpq}}\cos\left(\frac{p\pi}{a}x'\right)\cos\left(\frac{q\pi}{b}y'\right)e^{jk_{zpq}(z-z')}, \tag{C13}$$

where $k_{xp}=p\pi/a$, $k_{yq}=q\pi/b$, and $k_{zpq}^2=k_0^2-k_{xp}^2-k_{yq}^2$, p and q are integer but should not be zero at the same time.

Substituting the Eq. (C13) into Eq. (C11), the Green's function in hole is solved as

$$G^h = \sum_{p=0}^{\infty}\sum_{q=0}^{\infty} \frac{2j}{abk_{zpq}} e^{jk_{zpq}(z-z')}\cos\left(\frac{p\pi}{a}x\right) \times \cos\left(\frac{p\pi}{a}x'\right)\cos\left(\frac{q\pi}{b}y\right)\cos\left(\frac{q\pi}{b}y'\right). \tag{C14}$$

Considering that there are forward and backward waves in the waveguide, the Green's function should take the following form

$$G^h = \sum_{p=0}^{\infty}\sum_{q=0}^{\infty} \frac{2j}{abk_{zpq}} (e^{jk_{zpq}(z-z')} + e^{-jk_{zpq}(z-z')})\cos\left(\frac{p\pi}{a}x\right)\cos\left(\frac{p\pi}{a}x'\right) \times \cos\left(\frac{q\pi}{b}y\right)\cos\left(\frac{q\pi}{b}y'\right), \tag{C15}$$

where p and q are mode number of the mimicking surface plasmon wave in the holes. For TE_{01} mode, $p=0$, $q=1$

$$G^h = \frac{2j}{abk_{zh}}(e^{jk_{zh}(z-z')} + e^{-jk_{zh}(z-z')})\cos\left(\frac{\pi}{b}y\right)\cos\left(\frac{\pi}{b}y'\right), \tag{C16}$$

where $k_{zh}^2 = k_0^2 - (\pi/b)^2$.

APPENDIX D: BOUNDARY CONDITIONS AND COEFFICIENTS

The approach to match the boundary conditions is the same with that used in Appendix A.

At the surface of upper half space ($z=0$), in one period cell, the boundary conditions are

$$E_x^i + E_x^{ra} = E_x^h; \quad \int_{-D/2}^{D/2} H_y^i + \int_{-D/2}^{D/2} H_y^{ra} = DH_y^h.$$

At the surface of lower half space ($z=-h$), in one period cell, the boundary conditions are

$$E_x^{rb} = E_x^h; \quad \int_{-D/2}^{D/2} H_y^{rb} = DH_y^h.$$

After matching these boundary conditions, the coefficients B_{1mn}, B_2, B_3, and B_{4mn} can be obtained. Here, for simplicity we give the coefficients on the $y=0$ plane

$$B_{1mn} = \frac{a}{D}\mathrm{sinc}\left(\frac{k_x - k_{xm}}{2}a\right)E_0 + \frac{a}{D}(B_2 - B_3)\mathrm{sinc}\left(\frac{k_{xm}a}{2}\right),$$

$$B_2 = \frac{M_r M_p + M_h}{M_r M_p - M_h} e^{2jk_{zh}h} B_3,$$

$$B_3 = \frac{M_i - M_r M_p/\mathrm{sinc}\left(\frac{k_{xm}a}{2}\right)}{M_r M_p + M_h} \frac{\mathrm{sinc}\left(\frac{k_x - k_{xm}}{2}a\right)}{e^{2jk_{zh}h} - 1} E_0,$$

$$B_{4mn} = \frac{a}{D}(B_2 e^{-jk_{zh}h} - B_3 e^{jk_{zh}h}) e^{jk_{zmn}h}\,\mathrm{sinc}\left(\frac{k_{xm}a}{2}\right),$$

where $M_i = k_0$, $M_r = \frac{k_0^2}{k_{zmn}}$, $M_h = k_{zh}$, $M_p = \frac{a}{D}\Sigma_m \mathrm{sinc}^2(\frac{k_{xm}a}{2})$, and $E_0 = \frac{qk_x}{2\epsilon_0 u_0 k_z}(1-\beta^2)e^{-k^i z_0}$.

[1] R. Ulrich, Infrared Phys. **7**, 37 (1967).
[2] Chao-Chun Chen, IEEE Trans. Microwave Theory Tech. **18**, 627 (1970).
[3] Chao-Chun Chen, IEEE Trans. Microwave Theory Tech. **19**, 475 (1971).
[4] R. C. McPhedran, and D. Maystre, Appl. Phys. (Berlin) **14**, 1 (1977).
[5] L. Martín-Moreno and F. J. García-Vidal, J. Phys.: Condens. Matter **20**, 304214 (2008).
[6] W. L. Barnes, A. Dereux, and T. W. Ebbesen, Nature (London) **424**, 824 (2003).
[7] J. B. Pendry, L. Martin-Moreno, and F. J. Garcia-Vidal, Science **305**, 847 (2004).
[8] H.-T. Chen, W. J. Padilla, J. M. O. Zide, A. C. Gossard, A. J. Taylor, and R. D. Averitt, Nature (London) **444**, 597 (2006).
[9] D. R. Smith, J. B. Pendry, and M. C. K. Wiltshire, Science **305**, 788 (2004).
[10] F. J. García de Abajo and J. J. Sáenz, Phys. Rev. Lett. **95**, 233901 (2005).
[11] A. P. Hibbins, B. R. Evans, and J. R. Sambles, Science **308**, 670 (2005).
[12] T. W. Ebbesen, H. J. Lezec, H. F. Ghaemi, T. Thio, and P. A. Wolff, Nature (London) **391**, 667 (1998).
[13] S.-G. Liu *et al.*, Joint 32nd International Conference on Infrared and Millimeter Waves, 2007 and the 2007 15th International Conference on Terahertz Electronics, IRMMW-THz. (IEEE, 2007), Vol. 1, p. 899.
[14] L. Martín-Moreno, F. J. García-Vidal, H. J. Lezec, K. M. Pellerin, T. Thio, J. B. Pendry, and T. W. Ebbesen, Phys. Rev. Lett. **86**, 1114 (2001).
[15] H. Liu and P. Lalanne, Nature (London) **452**, 728 (2008).
[16] S. A. Darmanyan and A. V. Zayats, Phys. Rev. B **67**, 035424 (2003).
[17] F. J. García-Vidal, E. Moreno, J. A. Porto, and L. Martín-Moreno, Phys. Rev. Lett. **95**, 103901 (2005).
[18] T. Matsui, A. Agrawal, A. Nahata, and Z. V. Vardeny, Nature (London) **446**, 517 (2007).
[19] D. Schurig, J. J. Mock, B. J. Justice, S. A. Cummer, J. B. Pendry, A. F. Starr, and D. R. Smith, Science **314**, 977 (2006).
[20] Y.-M. Shin, J.-K. So, K.-H. Jang, J.-H. Won, A. Srivastava, and G.-S. Park, Appl. Phys. Lett. **90**, 031502 (2007).
[21] Y.-M. Shin, J.-K. So, K.-H. Jang, J.-H. Won, A. Srivastava, and G.-S. Park, Phys. Rev. Lett. **99**, 147402 (2007).
[22] J. T. Shen, P. B. Catrysse, and S. Fan, Phys. Rev. Lett. **94**, 197401 (2005).
[23] S. J. Smith and E. M. Purcell, Phys. Rev. **92**, 1069 (1953).
[24] G. T. D. Francia, Nuovo Cimento **61**, 1085 (1960).
[25] P. M. van den Berg, J. Opt. Soc. Am. **63**, 689 (1973).
[26] It has been proven by both computer simulation and analytical theory in the paper that the electromagnetic passing through the holes below cut-off frequency has no phase delay. From the point view of physics, the choice of electromagnetic penetration seems better than the term of transmission.
[27] It should be noticed here that the classical integral equation with relevant Green's functions [28,29] for each region, as the mathematical formulation of Huygens principle, can be used to solve the problem, it is not necessary to use Dyadic Green's function as claimed in [5].
[28] D. Ivanenko and A. Sokolov, *Classical Field Theory*, 2nd ed. (State Press, Moscow, USSR, 1951).
[29] I. M. Frank and I. E. Tamm, Reports of the USSR Academy of Sciences **14**, 107 (1937).
[30] M. Born and E. Wolf, *Principles of Optics*, 7th ed. (Cambridge University Press, Cambridge, UK, 1999).